Journal of Virology

Ebola Virus Modulates Transforming Growth Factor β Signaling and Cellular Markers of Mesenchyme-Like Transition in Hepatocytes

Jason Kindrachuk, Victoria Wahl-Jensen, David Safronetz, Brett Trost, Thomas Hoenen, Ryan Arsenault, Friederike Feldmann, Dawn Traynor, Elena Postnikova, Anthony Kusalik, Scott Napper, Joseph E. Blaney, Heinz Feldmann and Peter B. Jahrling

J. Virol. **2014, 88(17):9877. DOI: 10.1128/JVI.01410-14. Published Ahead of Print 18 June 2014.**

JVI Journals.ASM.org

Ebola Virus Modulates Transforming Growth Factor β Signaling and Cellular Markers of Mesenchyme-Like Transition in Hepatocytes

Jason Kindrachuk,[a,b] Victoria Wahl-Jensen,[b,h] David Safronetz,[c] Brett Trost,[d] Thomas Hoenen,[c] Ryan Arsenault,[e,f] Friederike Feldmann,[g] Dawn Traynor,[b] Elena Postnikova,[b] Anthony Kusalik,[d] Scott Napper,[e,f] Joseph E. Blaney,[a] Heinz Feldmann,[c] Peter B. Jahrling[a,b]

Emerging Viral Pathogens Section, National Institute of Allergy and Infectious Diseases, National Institutes of Health, Bethesda, Maryland, USA[a]; Integrated Research Facility, Division of Clinical Research, National Institute of Allergy and Infectious Diseases, National Institutes of Health, Frederick, Maryland, USA[b]; Laboratory of Virology, Division of Intramural Research, National Institute of Allergy and Infectious Diseases, National Institutes of Health, Hamilton, Montana, USA[c]; Department of Computer Science, University of Saskatchewan, Saskatoon, Saskatchewan, Canada[d]; Department of Biochemistry, University of Saskatchewan, Saskatoon, Saskatchewan, Canada[e]; Vaccine and Infectious Disease Organization, University of Saskatchewan, Saskatoon, Saskatchewan, Canada[f]; Rocky Mountain Veterinary Branch, Division of Intramural Research, National Institute of Allergy and Infectious Diseases, National Institutes of Health, Hamilton, Montana, USA[g]; National Biodefense Analysis and Countermeasures Center, Frederick, Maryland, USA[h]

ABSTRACT

Ebola virus (EBOV) causes a severe hemorrhagic disease in humans and nonhuman primates, with a median case fatality rate of 78.4%. Although EBOV is considered a public health concern, there is a relative paucity of information regarding the modulation of the functional host response during infection. We employed temporal kinome analysis to investigate the relative early, intermediate, and late host kinome responses to EBOV infection in human hepatocytes. Pathway overrepresentation analysis and functional network analysis of kinome data revealed that transforming growth factor (TGF-β)-mediated signaling responses were temporally modulated in response to EBOV infection. Upregulation of TGF-β signaling in the kinome data sets correlated with the upregulation of TGF-β secretion from EBOV-infected cells. Kinase inhibitors targeting TGF-β signaling, or additional cell receptors and downstream signaling pathway intermediates identified from our kinome analysis, also inhibited EBOV replication. Further, the inhibition of select cell signaling intermediates identified from our kinome analysis provided partial protection in a lethal model of EBOV infection. To gain perspective on the cellular consequence of TGF-β signaling modulation during EBOV infection, we assessed cellular markers associated with upregulation of TGF-β signaling. We observed upregulation of matrix metalloproteinase 9, N-cadherin, and fibronectin expression with concomitant reductions in the expression of E-cadherin and claudin-1, responses that are standard characteristics of an epithelium-to-mesenchyme-like transition. Additionally, we identified phosphorylation events downstream of TGF-β that may contribute to this process. From these observations, we propose a model for a broader role of TGF-β-mediated signaling responses in the pathogenesis of Ebola virus disease.

IMPORTANCE

Ebola virus (EBOV), formerly Zaire ebolavirus, causes a severe hemorrhagic disease in humans and nonhuman primates and is the most lethal Ebola virus species, with case fatality rates of up to 90%. Although EBOV is considered a worldwide concern, many questions remain regarding EBOV molecular pathogenesis. As it is appreciated that many cellular processes are regulated through kinase-mediated phosphorylation events, we employed temporal kinome analysis to investigate the functional responses of human hepatocytes to EBOV infection. Administration of kinase inhibitors targeting signaling pathway intermediates identified in our kinome analysis inhibited viral replication *in vitro* and reduced EBOV pathogenesis *in vivo*. Further analysis of our data also demonstrated that EBOV infection modulated TGF-β-mediated signaling responses and promoted "mesenchyme-like" phenotypic changes. Taken together, these results demonstrated that EBOV infection specifically modulates TGF-β-mediated signaling responses in epithelial cells and may have broader implications in EBOV pathogenesis.

Ebola virus (EBOV) is a filamentous, nonsegmented, single-stranded, negative-sense RNA virus. EBOV is the most lethal of the five members of the *Ebolavirus* genus, all of which cause Ebola virus disease (EVD), with a median case fatality rate of 78.4% (1). Although EVD outbreaks are sporadic, EBOV causes a severe hemorrhagic disease in humans and nonhuman primates (2). As a result of its high lethality and the potential for accidental introduction from regions where it is endemic to nonnative ones or intentional release for bioterrorism purposes, EBOV is considered a global health concern (2). Concerns regarding virus spread from rural to urban areas during the recent outbreak of EVD in Uganda (due to Sudan virus) and the continuing outbreak in Guinea, Liberia, and Sierra Leone (due to EBOV) have heightened fears regarding the introduction of these highly lethal viruses into densely populated areas (3, 4). These concerns have been further exacerbated by the importation of Marburg virus, a *Filoviridae* family member that also causes severe hemorrhagic fever, by tour-

Received 14 May 2014 Accepted 9 June 2014
Published ahead of print 18 June 2014
Editor: D. S. Lyles
Address correspondence to Jason Kindrachuk, kindrachuk.kenneth@nih.gov.
J.K. and V.W.-J. contributed equally to this publication.

doi:10.1128/JVI.01410-14

ists returning to the Netherlands and the United States from Uganda (5, 6). Although there has been considerable investigation into medical countermeasures for EBOV infection (7, 8), treatment is principally based on supportive care.

Clinical presentation of EVD (2, 9) includes gastrointestinal, respiratory, vascular, and neurological manifestations (10, 11). Hemorrhagic manifestations of EVD include petechiae and mucosal hemorrhage that arise during the peak of illness and are characterized by altered fluid distribution, hypotension, and aberrant coagulopathy (12, 13). Monocytes, macrophages, and dendritic cells are believed to be early targets of infection by the virus and play a central role in infection through the expression of proinflammatory and antiviral cytokines, including alpha interferon (IFN-α), interleukin-1 (IL-1), IL-6, IL-8, IL-12, tumor necrosis factor (TNF) family members, and coagulation factors (11, 13–18). Further, virus replication can be found in most major organs and cells of the endothelial, epithelial, and monocyte lineages in human and nonhuman primates (18–22). Although dysregulation of the vascular system and inflammatory response play key roles in EVD progression, the effect of EBOV infection on global cell signaling networks is largely uncharacterized.

Genome-wide expression studies have provided useful information regarding the host response to EBOV infection (23–25). For example, Kash et al. demonstrated that EBOV suppressed host antiviral responses, including Toll-like receptor (TLR)-, interferon (IFN) regulatory factor 3-, and protein kinase R (PKR)-mediated pathways in human hepatocytes (24). More recently, Wahl-Jensen and colleagues demonstrated that EBOV particle attachment and entry into human macrophages resulted in the induction of proinflammatory mediators, including interleukin (IL-6), IL-8, and tumor necrosis factor alpha (TNF-α), 1 h postinfection (p.i.) (25). While such studies of global gene expression have been informative, many questions remain regarding the molecular pathogenesis of EBOV infection. In addition, many cellular processes are regulated through posttranslational modification of host proteins that occur independently of changes in transcription or translation. Virtually all cell signaling processes are regulated by phosphotransfer reactions, and aberrant kinase activity has been implicated in a variety of host- and pathogen-mediated diseases (26). As a result, kinases are regarded as an attractive target for therapeutic intervention (27). Kinome profiling through global analysis of kinase abundance, activity, phosphorylation status, and substrate specificity provides a novel mechanism for investigating disease pathogenesis through the activation or repression of host cell signal transduction pathways (28). Recently, we have demonstrated the power of kinome analysis for characterizing molecular mechanisms of viral pathogenesis and for identifying specific cell signaling networks modulated during the course of infection (29).

The aim of this study was to investigate the temporal host kinome response to EBOV infection in human hepatocytes to identify specific cell signaling networks modulated during the course of infection. We employed HUH7 liver cells, a hepatoma cell line, as hepatocytes are targeted by EBOV during infection (20, 30) and HUH7 cells are permissive to EBOV infection (24). We determined the early, intermediate, and late host responses of EBOV-infected HUH7 cells compared to mock-infected cells through temporal kinome analysis. Pathway overrepresentation analysis (ORA) and functional network analysis were used to identify specific cell signaling responses that were modulated throughout the course of infection. Specifically, transforming growth factor beta (TGF-β)-mediated signaling responses were modulated in response to EBOV infection. The temporal upregulation of TGF-β-mediated signaling responses correlated with the enhanced secretion of TGF-β1 and vascular endothelial growth factor (VEGF) from EBOV-infected cells. In addition, *in vitro* kinase inhibitor assays targeting cell signaling intermediates identified from our kinome analysis confirmed the identity of specific downstream signaling pathways modulated during EBOV infection. Treatment with kinase inhibitors targeting these signaling pathways provided partial protection in a lethal EBOV model of infection, thereby validating and confirming the biological significance of the *in vitro* results while providing evidence of the power of this approach to rapidly identify therapeutic targets. To gain insight into the significance of TGF-β signaling modulation during EBOV infection, we assessed cellular markers associated with activation or upregulation of TGF-β signaling. The expression patterns of multiple cellular proteins were consistent with epithelium-to-mesenchyme transition (EMT). Based on these findings, we propose a role for TGF-β-mediated signaling responses and epithelium-to-mesenchyme-like transition during EBOV infection that may have broader implications in EVD pathogenesis.

MATERIALS AND METHODS

Cell and virus conditions. EBOV H.sapiens-tc/COD/1976/Mayinga (EBOV), green fluorescent protein (GFP)-expressing EBOV (for kinase inhibitor experiments), or mouse-adapted EBOV (for *in vivo* experiments) were used for all infections. For purified virus preparations, Vero E6 cells were infected with EBOV at a 1:1,000 dilution in Dulbecco's modified Eagle medium (DMEM) supplemented with 2% fetal bovine serum (FBS) and monitored daily for cytopathic effect (CPE). Cells subsequently were scraped, and supernatants were clarified by centrifugation at 3,000 rpm for 10 min. Supernatants then were pooled and overlaid over 20% sucrose solution, and virus was pelleted by ultracentrifugation at 25,000 rpm for 2 h. Supernatants were removed, and virus pellets were resuspended in DMEM supplemented with 10% FBS. All viral infections were performed at the National Institutes of Health Integrated Research Facility-Rocky Mountain Laboratories in Hamilton, MT, at biosafety level 4 (BSL4) in accordance with NIH/CDC Biosafety in Microbiological and Biomedical Laboratories guidelines, as well as in accordance with CDC Select Agent regulations (31). HUH7 cells (a kind gift from Hideki Ebihara), a human hepatoma cell line, were maintained in Dulbecco's minimal essential medium (DMEM) (Sigma-Aldrich) supplemented with 10% (vol/vol) heat-inactivated fetal bovine serum (FBS) and 2 mM L-glutamine. All cultures were maintained at 37°C in a humidified 5% (vol/vol) CO_2 incubator.

Chemical inhibitors. SB431542 and LY294002 were purchased from SelleckChem. Rottlerin and AG879 were purchased from Tocris. SU1498 was purchased from EMD. All other inhibitors were purchased from Enzo Life Sciences.

Antibodies. E-cadherin (Cell Signaling), N-cadherin (Cell Signaling), vimentin (Cell Signaling), β-catenin (Cell Signaling), claudin-1 (Cell Signaling), MMP9 (Cell Signaling), and fibronectin (Sigma-Aldrich) primary antibodies were used throughout this study for the detection of changes in EMT marker expression. Phospho-TAK1 (Cell Signaling), phospho-SMAD3 (Cell Signaling), phospho-JNK-1/2 (Cell Signaling), phospho-p38 (Cell Signaling), and phospho-ERK-1/2 (Cell Signaling) primary antibodies were used throughout this study for the detection of changes in protein phosphorylation. β-Tubulin (Cell Signaling) primary antibody was used as a control for protein loading.

Viral infection for kinome analysis. HUH7 cells were plated in 6-well plates and rested for 24 h prior to infection. Cells were infected with EBOV

at a multiplicity of infection (MOI) of 3 or mock infected with an equivalent volume of culture medium free of virus. Virus was incubated with host cells for 1 h at 37°C with periodic rocking. Following incubation, HUH7 cells were washed twice with phosphate-buffered saline (PBS) to remove unbound virus and replenished with fresh DMEM supplemented with 2% (vol/vol) FBS and incubated at 37°C. EBOV-infected and mock-infected cells were harvested at the appropriate time points (1, 6, and 24 h p.i.) for subsequent kinome analysis.

Kinome analysis. Design, construction, and application of the peptide arrays were based on a previously reported protocol, with the following modifications (32). EBOV-infected and mock-infected HUH7 cells were scraped and pelleted following infection, and cell lysates were prepared and incubated with human kinome arrays (JPT Technologies). Briefly, cell pellets were lysed with 100 μl of lysis buffer (20 mM Tris-HCl, pH 7.5, 150 mM NaCl, 1 mM EDTA, 1 mM ethylene glycol tetraacetic acid, 1% Triton X-100, 2.5 mM sodium pyrophosphate, 1 mM Na_3VO_4, 1 mM NaF, 1 μg/ml leupeptin, 1 μg/ml aprotinin, 1 mM phenylmethylsulfonyl fluoride) and incubated on ice for 10 min, followed by centrifugation to remove cell debris. A 70-μl aliquot of the cleared supernatant was mixed with 10 μl of activation mix (50% glycerol, 50 μM ATP, 60 mM $MgCl_2$, 0.05% Brij-35, and 0.25 mg/ml bovine serum albumin) and incubated on a kinome array for 2 h at 37°C. Kinome arrays subsequently were washed once with PBS containing 1% Triton X-100, followed by a single wash in distilled water (dH_2O). Peptide arrays were subjected to gamma irradiation to inactivate remaining virus (5 Mrad) and removed from the BSL4 laboratory according to approved standard operating protocols. Kinome arrays were submerged in PRO-Q Diamond phosphoprotein stain (Invitrogen) with gentle agitation in the dark for 1 h. Following staining, arrays were washed in destain (20% acetonitrile, 50 mM sodium acetate, pH 4.0 [Sigma-Aldrich]) 3× for 10 min/wash with the addition of fresh destain each time. A final wash was performed with dH_2O, placed in 50-ml conical tubes, and air dried for 20 min. Remaining moisture on the arrays was removed by centrifugation of the arrays at 300 × *g* for 3 min. Array images were acquired using an Axon 4000B microarray scanner at 532 to 560 nm with a 580-nm filter to detect dye fluorescence. Images were collected using GenePix 6.0 software (MDS). Signal intensity values were collected using GenePix 6.0 software (MDS) with the following settings: scanner saturation level 65535, background calculation done using the local feature background, signal mean and background mean intensity values were used for analysis, local background features exclude 2 pixels, and width of background set to 3 feature diameters. Intensity values for the spots and background were collected for each array.

Kinome data preprocessing. The specific responses of each peptide were calculated by subtracting background intensity from foreground intensity. The resulting data were transformed using the variance stabilization (*vsn*) model (33) to bring all of the arrays onto the same scale while alleviating the dependence between variance and mean estimators. In addition, for each of the 297 peptides in a single treatment, the intensities induced by the treatments were subtracted from the intensities from the time-matched biological control (i.e., HUH7 plus control media), and test statistics were calculated. Average intensities then were taken over the three transformed replicate intensities, and these values were subjected to hierarchical clustering analysis. Mathematical analysis of the data sets was performed as previously reported (32, 34).

Treatment-treatment variability analysis. Peptide phosphorylations were subjected to paired *t* tests to compare their signal intensities under one treatment condition to those under the control condition. Three tests were done for each peptide, as previously described (33).

Hierarchical clustering analysis. The preprocessed data were subjected to hierarchical clustering using the R function heatmap.2 to group treatments based on their kinome profiles. Each treatment vector was considered a singleton (i.e., a cluster with a single element) at the initial stage of the clustering. The distance metric and linkage method used were 1 − Pearson correlation and the McQuitty method, respectively (35). The hierarchical clustering was augmented by a heatmap that is also generated using the R function heatmap.2. The function converts the intensity values to statistical z-scores, and then the z-scores are coded as color (green/red) intensities. Green usually indicates a value lower than the means; red indicates a higher value.

Pathway overrepresentation analysis of differentially phosphorylated proteins. InnateDb (www.innatedb.com) is a publically available resource that predicts biological pathways related to the innate immune response of humans, mice, and bovines to microbial infection based on experimental fold change data sets (36). Pathways are assigned a probability (*P*) value based on the number of genes present for a particular pathway, as well as the degree to which they are differentially expressed or modified relative to a control condition. For our investigation, input data were limited to peptides that showed consistent responses across the biological replicates ($P < 0.05$) as well as statistically significant changes from the control condition ($P < 0.20$), as reported previously (32). Additionally, functional networks were created using ingenuity pathway analysis (IPA) software (Ingenuity Systems, Redwood City, CA). Proteins with known protein symbols and their corresponding phosphorylation values were uploaded and mapped to their corresponding protein objects in the IPA Knowledge Base. Networks of these proteins were algorithmically generated based on their connectivity and assigned a score. Proteins are represented as nodes, and the biological relationship between two nodes is represented as an edge (line). The intensity of the node color indicated the degree of up- or downregulation. Proteins in uncolored nodes were not identified as differentially expressed in our experiment and were integrated into the computationally generated networks on the basis of the evidence stored in the IPA knowledge database, indicating a relevance to this network.

Enzyme-linked immunosorbent assays. HUH7 cells were infected with EBOV or mock infected as described above. Cell supernatants from infected or mock-infected cells were harvested at 1, 6, or 24 h p.i. and exposed to gamma irradiation to inactivate remaining virus (5 Mrad) according to approved standard operating protocols. Following inactivation, supernatants were removed from the BSL4 conditions for subsequent analysis. The concentrations of 19 cytokines and chemokines in the supernatants were analyzed using a Millipore human 19-plex panel (Millipore). Supernatant samples were transferred to a 96-well plate and incubated with antibody-coated beads directed against different cytokines or chemokines. Following incubation, the beads were washed, incubated with anti-cytokine and anti-chemokine antibodies, and incubated with streptavidin-R-phycoerythrin (SAV/RPE). Beads were assayed on the Luminex 100/200 system (Bio-Rad, Hercules, CA). TGF-β1 and VEGF were measured using a human TGF-β1 Quantikine enzyme-linked immunosorbent assay (ELISA) kit and the human VEGF Quantikine ELISA kit (R&D Systems) by following the manufacturer's instructions. Detection of Th1/Th2/Th17 cytokines was assessed with the human Th1/Th2/Th17 cytokine multianalyte ELISArray kit (Qiagen). Experiments were done in duplicate and were repeated at least three times independently.

Kinase inhibitor assays. HUH7 cells were plated in 96-well plates in DMEM supplemented with 2% (vol/vol) FBS and rested for 24 h prior to infection. Cells were treated with kinase inhibitors (10 μM) for 1 h prior to infection with subsequent addition of GFP-expressing EBOV at an MOI of 3 or were mock infected with an equivalent fraction of culture medium free of any virus. The utility of EBOV-GFP as a screening tool for antiviral activity was previously reported (37). Infected cells were incubated at 37°C for 24 h. Cells were fixed in 10% neutral buffered formalin (NBF) for 24 h prior to removal from BSL4 conditions according to approved standard operating protocols and for an additional 24 h under BSL2 conditions with fresh 10% NBF. GFP signal was visualized on the Operetta high-content imaging system (PerkinElmer), and data were analyzed using Harmony software.

Cell viability assays. The effects of kinase inhibitors on HUH7 cell proliferation were evaluated using the WST-1 proliferation assay (Millipore). Briefly, HUH7 cells (2×10^4 cells) were plated and rested over-

night, followed by incubation with the various kinase inhibitors for 24 h. WST-1/ECS solution then was added at a ratio of 1:10 and incubated at 37°C for 2 h. Absorbance readings were acquired on a plate reader at a wavelength of 450 nm. Independent experiments were done in duplicate or triplicate and were repeated at least three times.

Animal infections. BALB/c mice (6 weeks of age) were obtained from Charles River Laboratories and housed in HEPA-filtered microisolator cage systems. Groups of 10 mice were infected with 1,000 50% lethal doses (LD_{50}; 10 focus-forming units [FFU]) of mouse-adapted EBOV by the intraperitoneal (i.p.) route. Kinase inhibitor treatments were delivered 1 h p.i. by intraperitoneal administration (1 or 5 mg/kg of body weight) (day 0) and were repeated daily until day 5. Mice were monitored for signs of disease, including ruffled fur, hunched posture, and weight loss, and survival for up to 21 days following infection. This study was carried out in strict accordance with the recommendations described in the *Guide for the Care and Use of Laboratory Animals* of the National Institutes of Health, the Office of Animal Welfare, and the United States Department of Agriculture (38). The Institutional Animal Care and Use Committee (IACUC) at the Rocky Mountain Laboratories (RML) approved all animal work. The RML is accredited by the American Association for Accreditation of Laboratory Animal Care (PHS/OLAW Animal Welfare Assurance A4149-01). All procedures were carried out under ketamine anesthesia by trained personnel under the supervision of veterinary staff, and all efforts were made to ensure the welfare of the animals and to minimize their suffering. Early endpoint criteria, as specified by the RML IACUC-approved monitoring parameters, were used to determine when animals should be humanely euthanized.

Western blot analysis. HUH7 cells were mock infected or infected with EBOV as described above. Cells from infected or mock-infected cells were harvested at 1, 6, or 24 h p.i. and lysed in SDS loading buffer without bromophenol blue (200 mM Tris-HCl, pH 6.8, 8% SDS, 40% glycerol, 4% β-mercaptoethanol, 50 mM EDTA) and exposed to gamma irradiation to inactivate remaining virus (5 Mrad) according to approved standard operating procedures. Following inactivation, supernatants were removed from the BSL4 conditions for subsequent analysis. Protein concentration was determined using the bicinchoninic acid (BCA) protein assay kit (Pierce) according to the manufacturer's instructions. Equivalent amounts of total cell lysates were separated on 4% to 12% Bis-Tris gradient gels (Invitrogen) and wet transferred onto polyvinylidene difluoride membranes (Bio-Rad). Membranes were blocked (5% [wt/vol] nonfat milk or 5% [wt/vol] BSA in TBS-Tween20 [0.5%, wt/vol]) prior to incubation with primary antibodies and subsequent detection with appropriate horseradish peroxidase-conjugated secondary antibodies (Pierce). Complexes were visualized using SuperSignal West Femto chemiluminescent substrate (Pierce). Images were acquired using a Syngene G:Box Chemi (Syngene).

Conditioned medium experiments. HUH7 cells were infected with EBOV-GFP or mock infected as described above. Cell supernatants from infected or mock-infected cells were harvested at 24 h p.i. Cells were scraped into supernatant, and then supernatants were clarified by centrifugation (1,000 rpm, 4°C, 20 min). Clarified supernatants then were ultracentrifuged to directly pellet virus and obtain virus-free conditioned media. Clarified supernatants were spun at 28,000 rpm for 1.5 h at 4°C in the SW41 rotor of a Beckman Coulter ultracentrifuge. Virus-free supernatants subsequently were diluted 1:1 with fresh EGM-2 media (Lonza, Walkersville, MD) and incubated with fresh human umbilical vein endothelial cells (HUVECs) for 24 h. Removal of EBOV-GFP was verified by imaging for GFP production in conditioned medium-treated HUVECs. Cells from infected or mock-infected cells were harvested, lysed in SDS loading buffer without bromophenol blue (200 mM Tris-HCl, pH 6.8, 8% SDS, 40% glycerol, 4% β-mercaptoethanol, 50 mM EDTA), and boiled for 10 min. VE-cadherin expression was examined through Western blot analysis as described above.

RESULTS

Temporal kinome analysis of cell signaling responses modulated by EBOV infection. Previously, we reported the utility of kinome analysis with peptide arrays for investigating host signaling responses to West African and Congo Basin monkeypox virus (29). Here, we employed a similar strategy to investigate host-cell signaling responses to EBOV infection. EBOV infection of HUH7 human liver cells was employed, as hepatocytes are a target for EBOV infection and do not undergo apoptosis following EBOV infection (24). Cells were infected at a multiplicity of infection (MOI) of 3 with EBOV and harvested throughout the course of infection, along with time-matched, mock-infected control cells, for kinome analysis with peptide arrays. Kinome analysis with peptide arrays relies on phosphotransfer from active kinases in a cell lysate to specific kinase targets (peptides) on the arrays and the subsequent identification and quantitation of these phosphorylation events. Our arrays contained 300 unique peptides representing key phosphorylation events from a broad spectrum of cell signaling pathways and processes. In agreement with previous investigations, EBOV infection of HUH7 cells did not result in induction of apoptosis (data not shown). The kinome data were extracted from the arrays and analyzed using the Platform for Intelligent, Integrated Kinome Analysis (PIIKA) software tool (32, 34). Data sets representing EBOV-infected cells clustered sequentially with the mock-infected 24-h and 1-h samples following hierarchical cluster analysis (Fig. 1A). Additional cluster analysis using PIIKA revealed that biological subtraction of the mock-infected control kinome data sets from their respective time-matched EBOV-infected data sets resulted in stronger clustering and a higher degree of similarity in host kinome responses between the 1-h p.i. and 24-h p.i. time points than the 6-h p.i. time point (Fig. 1B). Principal component analysis of the kinome data demonstrated almost complete separation of the mock- and EBOV-infected data sets into two individual clusters (Fig. 1C). These results suggested some level of conservation in the host responses to EBOV infection between the 1- and 24-h p.i. time points.

To gain biological insight into the nature of the host response to EBOV infection and, in particular, the nature of the conserved host response found between the 1- and 24-h p.i. data sets, we first utilized functional network analysis with the Ingenuity Pathway Analysis (IPA) software suite. TGF-β and TGF-β signaling pathway intermediates occupied central positions in both the 1- and 24-h p.i. networks but were absent from the 6-h p.i. network (Fig. 2A to C). To provide additional perspective on the specific cell signaling networks that were modulated during these time points, we performed pathway overrepresentation analysis (ORA) with the online software InnateDB (39, 40) (Table 1). Upregulated TGF-β-mediated signaling responses were found to be overrepresented at 1 and 24 h p.i. (Table 1). As with the functional network analysis, TGF-β-related signaling responses were absent from the 6-h p.i. signaling pathway analysis. As exogenous molecules within the virus preparation could have modulatory effects on host signaling pathways, supplemental experiments were performed using purified EBOV. Although the presence of exogenous molecules in the original viral preparation could have affected the activation state of host signaling networks at the 1-h p.i. time point, infection of cells with purified EBOV resulted in the upregulation of TGF-β-mediated signaling responses, which were highly overrepresented at 24 h p.i. These data further corrobo-

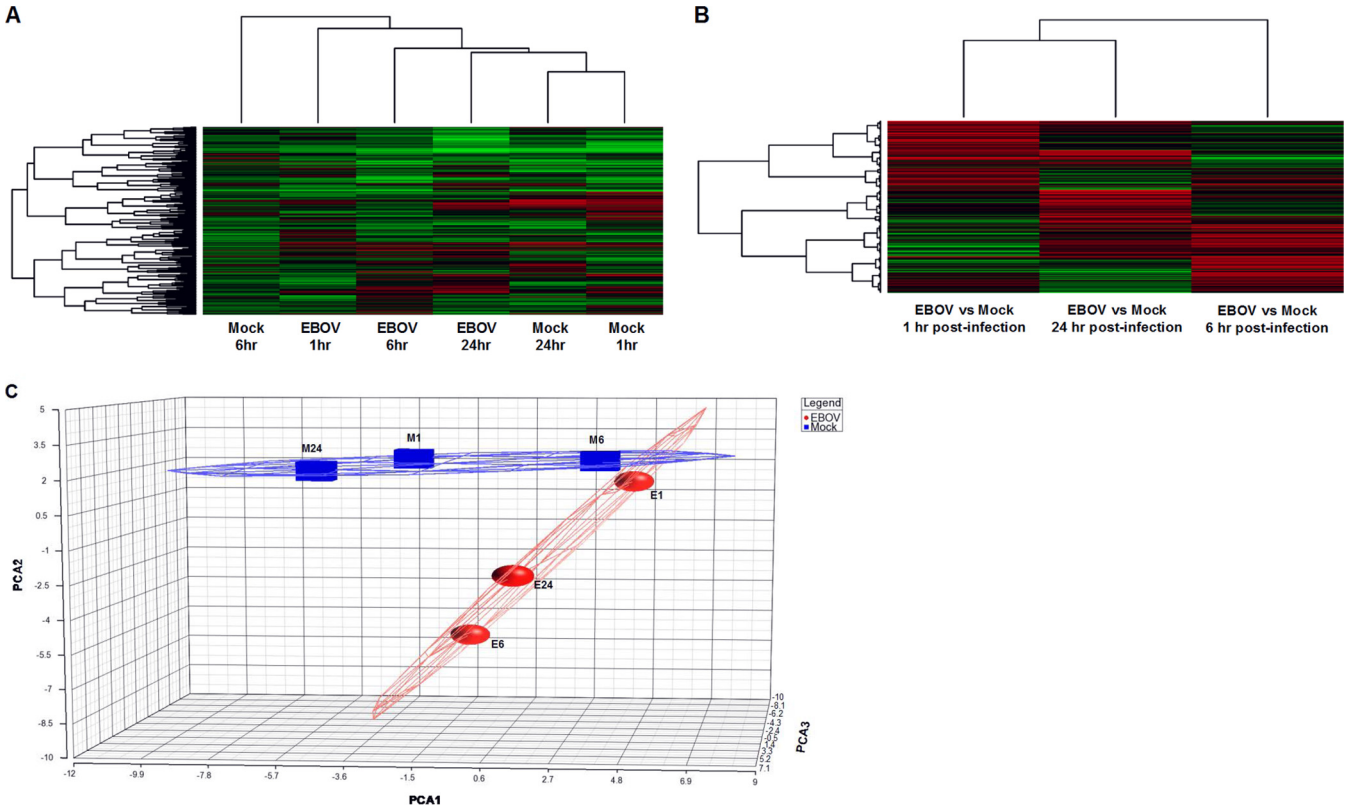

FIG 1 Heatmaps and hierarchical clustering of host kinome responses to EBOV infection. Peptide phosphorylation was assessed by densitometry, scaled, and normalized using GeneSpring 6.0 software. For hierarchical clustering, 1 − Pearson correlation coefficient was used as the distance metric, and the McQuitty method was used as the linkage method. (A) Hierarchical clustering of the EBOV-infected kinome data sets alongside the mock-infected control data sets. (B) Cluster analysis of the EBOV-infected kinome data sets following background subtraction of the time-matched mock-infected control data sets. Spots demonstrating a significant differential phosphorylation between the EBOV-infected and mock-infected control were compiled into a data set for each time point for comparative analysis. The lines at the top of the heatmap indicate the relative similarity between the conditions as listed along the bottom edge of the heatmap. Line length indicates the degree of similarity, with shorter lines equating to stronger similarity. The lines on the left side of the heatmap indicate the relative similarity in signal between the 300 individual peptide targets on the arrays. (C) Principal component analysis of the mock- and EBOV-infected kinome data sets.

rated our observations that EBOV infection modulated TGF-β-mediated signaling responses in hepatocytes (Table 2). Thus, TGF-β-related signaling likely comprised an important biological response in EBOV-infected hepatocytes, warranting further functional analysis of the role of TGF-β in the molecular pathogenesis of EBOV.

The induction of TGF-β secretion in EBOV-infected cells correlates with the activation of TGF-β signaling predicted by pathway ORA. To further investigate the role of the TGF-β signaling pathway in EBOV-infected hepatocytes, we assessed temporal TGF-β secretion from the EBOV-infected cells. Supernatants were collected throughout the course of infection from the mock- and EBOV-infected cells and screened for TGF-β secretion by enzyme-linked immunosorbent assay (ELISA).

ELISA of the HUH7 cell supernatants demonstrated significant increases in TGF-β secretion from the EBOV-infected cells compared to the mock controls at both 1 and 24 h p.i. but not at the 6-h time point (Fig. 3A). These results were corroborated by the upregulation of TGF-β signaling responses identified in our pathway ORA. As TGF-β can induce VEGF release from epithelial cells (41, 42) and multiple VEGF-mediated signaling pathways were upregulated by EBOV 1 h p.i., we also assessed VEGF secretion. As expected, VEGF secretion was significantly upregulated at 1 h p.i. (Fig. 3B). Interestingly, VEGF secretion also was significantly upregulated at 24 h p.i. We also observed increased secretion of monocyte chemoattractant protein 1 (MCP-1) and IL-8 at 1 h p.i. and 24 h p.i., respectively (data not shown).

Taken together, the patterns of growth factor secretion from the EBOV-infected HUH7 cells and, in particular, TGF-β secretion correlated with the observed overrepresentation of upregulated signaling responses found in our pathway analysis.

Selective modulation of signaling networks identified from kinome analysis decreases EVD severity *in vivo*. To gain further insight into the relationship between host kinases and the progression of EBOV infection in hepatocytes, we assessed the functional role of specific host kinases during infection. We first examined the effects of various inhibitors of tyrosine kinase cell surface receptors on EBOV infection. Importantly, all kinase inhibitors had negligible effects on cell proliferation (Fig. 4). Based on the overrepresentation of TGF-β signaling events and, to a lesser extent, VEGF and nerve growth factor (NGF)-mediated signaling, we focused on these cell receptors. In addition, we also focused on downstream signaling events conserved across these signaling networks (including phosphoinositide 3-kinase/AKT [PI3K/AKT], protein kinase C [PKC], and mitogen-activated protein kinase/extracellular signal-regulated protein kinase [MAPK/ERK] signal-

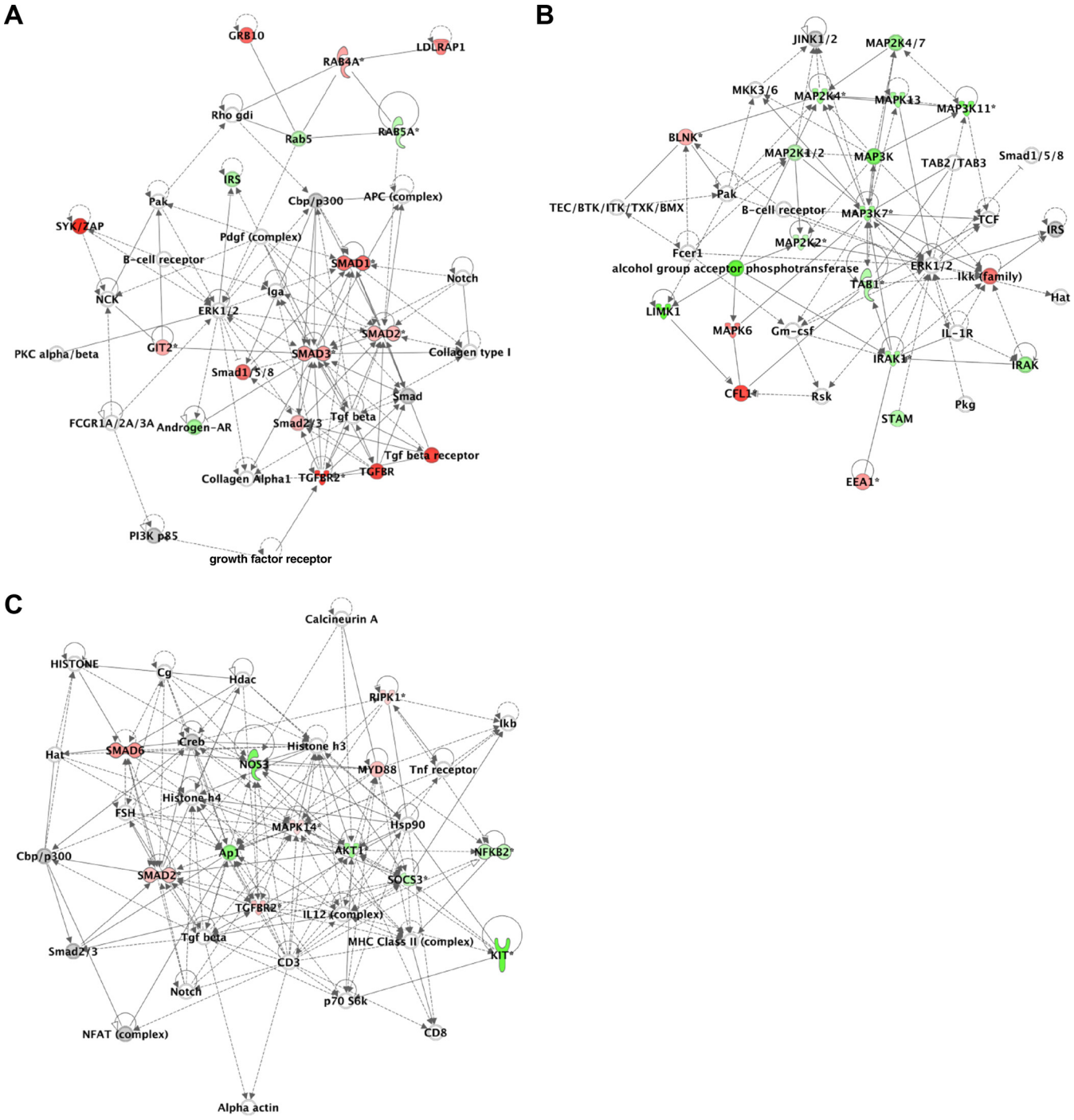

FIG 2 Functional network analysis of EBOV-infected hepatocyte kinome responses. Functional network analysis was performed using the IPA software suite. Each network represents the top functional network for the respective time point. (A) Responses at 1 h p.i., including embryonic development, organismal development, and cardiovascular system development and function. (B) Responses at 6 h p.i., including posttranslational modification, cell signaling, and cellular assembly and organization. (C) Responses at 24 h p.i., including cell death and survival, cellular development, and hematological system development and function.

ing). This choice was further supported by our observation that phosphorylation of signaling intermediates from the PI3K/AKT signaling pathway (PDK1 and PIK3R1), the MAPK/ERK signaling pathway (p38 MAPK, MEK1, Raf, and JNK), and PKC all were increased in the EBOV-infected kinome data sets compared to the mock-infected controls. Administration of kinase inhibitors targeting TGF-β (SB431542), NGF (AG879), PI3K/AKT (LY294002; wortmannin), and PKC signaling (rottlerin; GF109203X) retained the strongest inhibitory activity against *in vitro* EBOV infection when added before (−1 h) or after (+4 h) infection, whereas little

TABLE 1 InnateDB analysis of temporal kinome datasets from EBOV-infected HUH7 cells[a]

Description, regulation status, and modulation time point	*P* value	
	Upregulated	Downregulated
1 h p.i.		
Upregulated		
TGF-β receptor signaling	0.005	1.00
TGF-β signaling pathway	0.01	1.00
Negative feedback regulation of TGF-β superfamily signaling pathway by R-SMAD degradation (TGF-β superfamily signaling pathway [canonical])	0.03	1.00
TGF-β superfamily signaling pathway (canonical)	0.03	1.00
Endocytosis	0.07	0.96
BMP signaling pathway (TGF-β BMP Diagram [molecular variation])	0.08	1.00
Gene expression of SMAD6/7 by R-SMAD:SMAD4 (TGF-β superfamily signaling pathway [canonical])	0.08	1.00
Gene expression of SMAD7 by R-SMAD:SMAD4 (TGF-β superfamily signaling pathway [canonical])	0.08	1.00
Negative feedback regulation pathway of TGF-β superfamily signaling by (binding of smad6/7 and TGF-β receptor I) (TGF-β superfamily signaling pathway [canonical])	0.08	1.00
Negative regulation of transcription by R-SMAD:SMAD4 in TGF-β superfamily signaling pathway (TGF-β superfamily signaling pathway [canonical])	0.08	1.00
Signaling by TGF-β	0.08	1.00
TGF-β signaling pathway	0.08	1.00
Downregulated		
Hepatitis C	1.00	0.03
Toxoplasmosis	1.00	0.03
P53 signaling pathway	0.99	0.05
Amyotrophic lateral sclerosis	1.00	0.06
Caspase cascade in apoptosis	1.00	0.06
Cyclins and cell cycle regulation	1.00	0.06
FoxO family signaling	1.00	0.06
Renal cell carcinoma	1.00	0.06
T cell receptor signaling pathway	1.00	0.06
Pathways in cancer	0.97	0.08
Small cell lung cancer	0.98	0.1
TNFR1 signaling pathway (TNFR1 signaling pathway)	0.98	0.1
Toll-like receptor signaling pathway	0.98	0.1
6 h p.i.		
Upregulated		
ATF-2 transcription factor network	0.02	1.00
Regulation of nuclear beta catenin signaling and target gene transcription	0.02	1.00
Prolactin	0.04	0.62
EPO signaling pathway	0.06	0.75
Calcium signaling pathway	0.08	1.00
Coregulation of androgen receptor activity	0.08	0.87
LIF signaling pathway (LIF signaling [JAK1 JAK2 STAT3])	0.08	1.00
Androgen receptor	0.09	0.52
IL-6	0.1	0.56
RANKL	0.1	0.56
Leptin	0.1	0.59
Downregulated		
Insulin receptor signaling (insulin receptor signaling)	0.95	0.004
mTOR signaling pathway	1.00	0.01
IGF-1 signaling pathway (IGF1 signaling pathway)	0.93	0.01
AKT (PKB) activation signaling (IGF1 signaling pathway)	1.00	0.02
B cell survival pathway	1.00	0.02
CD28-dependent PI3K/Akt signaling	1.00	0.02
FGF signaling pathway	1.00	0.02
PTEN-dependent cell cycle arrest and apoptosis	1.00	0.02
Regulation of bad phosphorylation	1.00	0.02
IGF-1 receptor and longevity	1.00	0.02
Trk receptor signaling mediated by PI3K and PLC-gamma	1.00	0.02
IGF-1 pathway	1.00	0.03
Phospholipids as signaling intermediaries	0.90	0.03
Role of ERK5 in neuronal survival pathway	0.90	0.03

(Continued on following page)

TABLE 1 (Continued)

Description, regulation status, and modulation time point	*P* value	
	Upregulated	Downregulated
T cell receptor signaling pathway (CD4 T cell receptor signaling)	0.78	0.03
Aldosterone-regulated sodium reabsorption	1.00	0.05
C-MYB transcription factor network	1.00	0.05
Carbohydrate digestion and absorption	1.00	0.05
Costimulation by the CD28 family	1.00	0.05
Ctcf (first multivalent nuclear factor)	1.00	0.05
mTOR signaling pathway	1.00	0.05
Plasma membrane estrogen receptor signaling	1.00	0.05
Reelin signaling pathway	1.00	0.05
Role of nicotinic acetylcholine receptors in the regulation of apoptosis	1.00	0.05
Skeletal muscle hypertrophy is regulated via akt-mTOR pathway	1.00	0.05
Tie2 signaling	1.00	0.05
Chronic myeloid leukemia	0.91	0.06
Endometrial cancer	0.55	0.07
Non-small-cell lung cancer	0.55	0.07
T cell receptor signaling (PLC-gamma, PKC, Ras, and IKK-NF-κB cascade), CD4 T cell receptor signaling (NF-κB cascade)	0.83	0.07
Nfat and hypertrophy of the heart	1.00	0.07
Transcription factor creb and its extracellular signals	0.84	0.07
Colorectal cancer	0.69	0.07
IL-2 receptor beta chain in T cell activation	0.69	0.07
Natural killer cell-mediated cytotoxicity	0.69	0.07
Insulin signaling pathway	0.99	0.10
T cell receptor signaling pathway	0.78	0.10
24 h p.i.		
Upregulated		
Signaling by TGF-β	0.02	1.00
Gene expression of SOCS1 by STAT dimer (JAK-STAT pathway and regulation pathway Diagram)	0.06	0.96
Neurotrophic factor-mediated Trk receptor signaling	0.06	0.96
Erk1/Erk2 MAPK signaling pathway	0.08	0.88
TGF-β signaling pathway	0.08	1.00
Non-small-cell lung cancer	0.09	0.78
Downregulated		
TNFR1 signaling pathway (TNFR1 signaling pathway)	0.95	0.04
BCR	0.85	0.04
Epithelial cell signaling in *Helicobacter pylori* infection	0.87	0.04
Agrin in postsynaptic differentiation	1.00	0.06
Apoptotic signaling in response to DNA damage	1.00	0.06
Primary immunodeficiency	1.00	0.06
TAK1 activates NF-κB by phosphorylation and activation of IKK complex	1.00	0.06
FoxO family signaling	0.84	0.08
IL-4 signaling pathway	0.84	0.08
Integrin-linked kinase signaling	1.00	0.08
P53 signaling pathway	1.00	0.08
Shigellosis	1.00	0.08
IL-2 signaling events mediated by PI3K	0.93	0.09
TWEAK	1.00	0.09

[a] InnateDB is a publically available pathway analysis tool. Based on levels of differential expression or phosphorylation, InnateDB is able to predict pathways that are consistent with the experimental data. Pathways are assigned a probability (*P*) value based on the number of proteins present for a particular pathway. It also provides the number of uploaded pathways associated with a particular pathway as well as the subset of individual proteins that are differentially phosphorylated.

or no effect was observed after administration of the VEGFR inhibitor SU1498 (Fig. 4). This suggested that the role of VEGF induction in EBOV-infected hepatocytes was largely independent of direct activation of the VEGF receptor.

Taken together, our *in vitro* data strongly suggested that EBOV infection resulted in the selective modulation of specific cell signaling pathways, in particular those mediated by TGF-β. The kinase inhibitor experiments provided corroborating evidence that particular signaling pathways, or intermediates, were selectively and temporally modulated during EBOV infection, including TGF-β, NGF, PI3K/AKT, and PKC signaling events. If activation of these signaling pathways is a requirement for EBOV infection and replication, then selective inhibition of these cellular responses would be anticipated to reduce the lethality in an EBOV animal model. To address this, we evaluated the efficacy of SU1498 (VEGFR2), AG879 (TrkA), SB431542 (TGFβRII),

TABLE 2 InnateDB analysis of kinome datasets from HUH7 cells infected with purified EBOV

Pathway name or description	Upregulated *P* value	Proteins in pathway from analysis
HIV-1 nef (negative effector of fas and TNF)	0.01	BCL2, BID, CHUK, MDM2, PAK2, PTK2, RELA, TRAF2
Downregulation of TGF-β receptor signaling	0.01	SMAD2, TGFBR1, TGFBR2
TGF-β receptor signaling activates SMADs	0.01	SMAD2, TGFBR1, TGFBR2
Glypican 1 network	0.02	FLT1, SMAD2, TGFBR1, TGFBR2
Agrin in postsynaptic differentiation	0.02	EGFR, GIT2, JUN, PAK2, PAK4, PTK2, PXN
Alpha4 beta1 integrin signaling events	0.04	PRKACA, PTK2, PTK2B, PXN, YWHAZ
M-calpain and friends in cell motility	0.04	EGFR, MAP2K2, PTK2, PXN, SHC1
TGF-β signaling pathway	0.04	CDH1, SMAD2, TAB1, TGFBR1, TGFBR2
Ctcf (first multivalent nuclear factor)	0.06	CDKN1B, MDM2, MTOR, PIK3R1, PTEN, RPS6KB1, SMAD1, TGFBR1, TGFBR2
Cell cycle	0.08	CDK1, CDK4, CDKN1B, MDM2, SMAD2, YWHAZ
Chronic myeloid leukemia	0.09	ARAF, BRAF, CDK4, CDKN1B, CHUK, MAP2K2, MDM2, PIK3R1, RELA, SHC1, SHC3, STAT5B, TGFBR1, TGFBR2
Fc-epsilon receptor I signaling in mast cells	0.09	CHUK, FOS, JUN, LYN, MAP2K2, MAP2K4, NFATC2, PAK2, PIK3R1, PTK2, PXN, RELA, SHC1, SYK
AKT phosphorylates targets in the cytosol	0.09	CDKN1B, CHUK, MDM2
Alk in cardiac myocytes	0.09	SMAD1, TGFBR1, TGFBR2
Apoptotic signaling in response to DNA damage	0.09	BAX, BCL2, BID
C-MYB transcription factor network	0.09	BCL2, CDKN1B, KIT
Cell-to-cell adhesion signaling	0.09	CDH1, PTK2, PXN
FAS (CD95) signaling pathway	0.09	BID, CHUK, SYK
FCGR activation	0.09	HCK, LYN, SYK
GPCR adenosine A2A receptor signaling pathway	0.09	BRAF, MAP2K2, PRKACA
Integrin alphaIIb beta3 signaling	0.09	PTK2, SHC1, SYK
Melanocyte development and pigmentation pathway	0.09	BCL2, KIT, MAP2K2
Melanogenesis	0.09	KIT, MAP2K2, PRKACA
P53 signaling pathway	0.09	BCL2, CDK4, MDM2
Prion diseases	0.09	BAX, MAP2K2, PRKACA
Regulation of actin dynamics for phagocytic cup formation	0.09	LIMK1, PTK2, SYK
Role of mitochondria in apoptotic signaling	0.09	BAX, BCL2, BID
TGF-β receptor signaling in EMT	0.09	RHOA, TGFBR1, TGFBR2
uCalpain and friends in cell spread	0.09	PTK2, PXN, RHOA
Validated targets of C-MYC transcriptional repression	0.09	BCL2, CDKN1B, PDGFRB
a4b7 integrin signaling	0.09	PTK2, PXN, RHOA

LY294002 (PI3K), and rottlerin (PKC) to protect mice against a mouse-adapted strain of EBOV (43). Although the selective inhibition of the VEGF receptor had minimal inhibitory activity against EBOV infection *in vitro*, we also tested the VEGF receptor inhibitor SU1498, as VEGF secretion was significantly induced in EBOV-infected hepatocytes (Fig. 3B) and because of the observed upregulation of VEGF-mediated signaling events. Further, the activation of TGF-β signaling events in epithelial cells can induce VEGF secretion (41, 42). Groups of 10 mice were infected with 1,000 LD_{50} of mouse-adapted EBOV by the i.p. route. Kinase inhibitors were administered at 1 h postinfection (day 0) and then once daily until day 5 and were delivered by i.p. administration. Mice were monitored for signs of disease and survival for up to 21 days following infection.

All mice treated with vehicle alone succumbed to infection by day 7 p.i. Treatment with SU1498 (VEGFR2) or SB431542 (TGF-βRII) resulted in 20% survival at 5 mg/kg (Fig. 5). These results were consistent with our hypothesis that TGF-β and VEGF signaling were modulated during the course of EBOV infection. Further, administration of AG879 or SB431542 at 1 mg/kg resulted in 20% protection. Collectively, these results suggest that the pathogenesis of EBOV infection is related to the selective modulation of VEGF, NGF, and TGF-β signaling pathways. Further, administration of LY294002 (PI3K) or rottlerin (PKC) at 1 mg/kg conferred 40% and 30% protection from EBOV infection, respectively. These protective effects were shown to be significant for all of the inhibitors tested by the Mantel-Cox test and confirmed that the modulation of these signaling pathways during EBOV infection contribute to pathogenesis *in vivo*. All surviving mice were observed to be improved and gaining weight by 10 days p.i. These results confirm for the first time that EBOV infection results in the selective modulation of the TGF-β and VEGF signaling pathways and downstream PI3K and PKC signaling.

EBOV infection results in the modulation of expression of promesenchyme cellular markers. System-level analysis of the EBOV-infected kinome data sets demonstrated that upregulated TGF-β-mediated signaling responses were overrepresented at both 1 and 24 h p.i. and that TGF-β formed central cores of functional networks at these time points (Fig. 2 and Table 1). These results correlated with the significant upregulation of TGF-β secretion from infected cells and the inhibitory activity of selective TGFBRI antagonists on EBOV infection *in vitro* and *in vivo*. It also has been demonstrated that TGF-β induces an EMT state in hepatocytes to a fibroblast-type phenotype (44, 45). Thus, we sought to identify the potential cellular consequences for the upregulation of TGF-β signaling in EBOV-infected hepatocytes. TGF-β is a

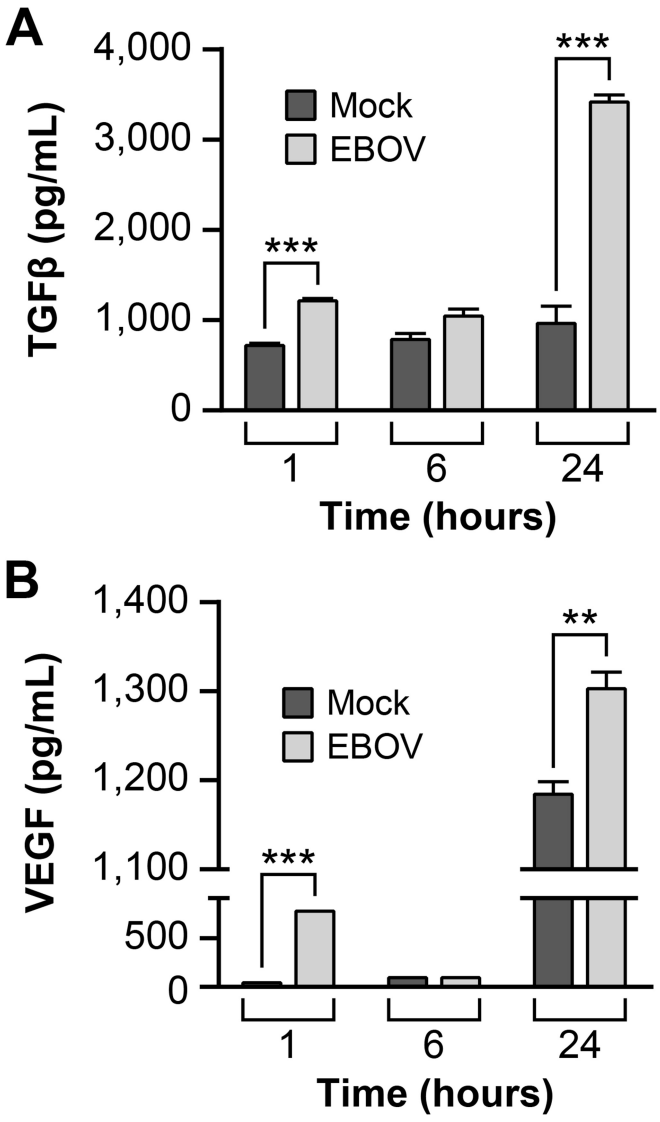

FIG 3 ELISA of secreted factors from EBOV-infected hepatocytes. HUH7 cells were infected with EBOV at an MOI of 3, and supernatants were collected at the indicated time points. The data presented represent the cytokines or chemokines that had measurable values compared to medium-only controls. Data are representative of three independent experiments ± standard deviations (SD).

pleiotropic molecule that has roles in the regulation of cell proliferation, differentiation, migration, wound healing, and immune responses (46). The influence of TGF-β on microbial pathogenesis has been described for a broad range of viruses, including influenza A virus, human immunodeficiency virus 1, and hepatitis B and C viruses (46). TGF-β treatment enhances phenotypic transformation of infected epithelial cells through EMT (47). This transformation is characterized by the disassembly of adherens junctions and tight junctions (48). Specific molecular characteristics include repression of E-cadherin, claudin-1, and β-catenin expression and the induction of the mesenchyme cytoskeletal proteins N-cadherin and vimentin, matrix metalloproteinase 9 (MMP9), and fibronectin (48). Viral infection can modulate the expression of cellular markers of EMT (49). We examined the effects of EBOV infection on common cellular markers of mesenchyme-like transition in an attempt to shed light on the effect of TGF-β modulation in EBOV-infected cells. EBOV infection resulted in downregulation of both E-cadherin and claudin-1 compared to levels for mock-infected cells (Fig. 6). In contrast, the expression of N-cadherin, MMP9, and fibronectin was increased 24 h following EBOV infection. Changes in the expression levels of these proteins were similar to those previously reported for cells undergoing EMT (47, 50). The modulation of these EMT markers was dependent on viral entry and/or replication, as EBOV-like particles constructed from VP40 or VP40 and $GP_{1,2}$ viral proteins and added exogenously to HUH7 cells had no effect on either E-cadherin or claudin-1 compared to mock-infected cells (Fig. 7). We also compared the effect of TGF-β stimulation of hepatocytes to mock-infected and EBOV-infected cells on a subset of EMT markers. As TGF-β and VEGF secretion were significantly increased in EBOV-infected hepatocytes, we next examined the effect of factors secreted from EBOV-infected HUH7 cells on endothelial cells. Treatment of HUVECs with virion-free conditioned media from EBOV-infected HUH7 cells resulted in the repression of VE-cadherin expression (Fig. 8).

As EBOV infection resulted in the induction of an EMT-like phenomenon in infected HUH7 cells, we next sought to identify signaling events downstream of the TGF-β receptors that help mediate these events. Western blot analysis was performed with phospho-antibodies against key signaling intermediates from the TGF-β signaling pathway that previously have been implicated in EMT potentiation. We analyzed the phosphorylation states of TAK1 (Thr187), SMAD3 (Ser423/Ser425), ERK1/2 (Thr202/Tyr204), p38 MAPK (Thr180/Tyr182), and JNK (Thr183). Our analysis demonstrated increases in phosphorylation of ERK1/2, p38 MAPK, SMAD3, and TAK1 in EBOV-infected cells 24 h p.i. (Fig. 9). In contrast, phosphorylation of JNK was decreased in EBOV-infected cells.

Thus, infection of hepatocytes with EBOV results in the modulation of specific cellular markers of epithelial cells that include decreased cell-to-cell contact, downregulated expression of cell adhesion molecules, and increased expression of fibrogenic molecules. In addition, the overall trends of these phenotypic changes mimicked those of TGF-β treatment. Further, Western blot analysis of signaling pathway intermediates suggest that EBOV infection results in the activation of ERK1/2, p38 MAPK, SMAD3, and TAK1 through increased phosphorylation downstream of the TGF-β receptor.

DISCUSSION

EBOV is one of the deadliest human pathogens, causing severe hemorrhagic fever with high case fatality rates (2, 51). Although there have been extensive studies of the pathological response to EBOV infection in animal models and EBOV exhibits a broad cell tropism (19–22, 52–56), there is a relative paucity of information regarding molecular pathogenesis beyond primary interactions between the virus and target cells. Global host-response surveys through genomic or proteomic techniques have been routinely employed to characterize infectious disease pathogenesis at the cellular level. Here, we employed kinomics along with system-level analysis to characterize the functional, global activation state of host kinases and cell signaling networks during EBOV infection of hepatocytes, a cell type targeted by EBOV.

We have demonstrated that EBOV infection of hepatocytes

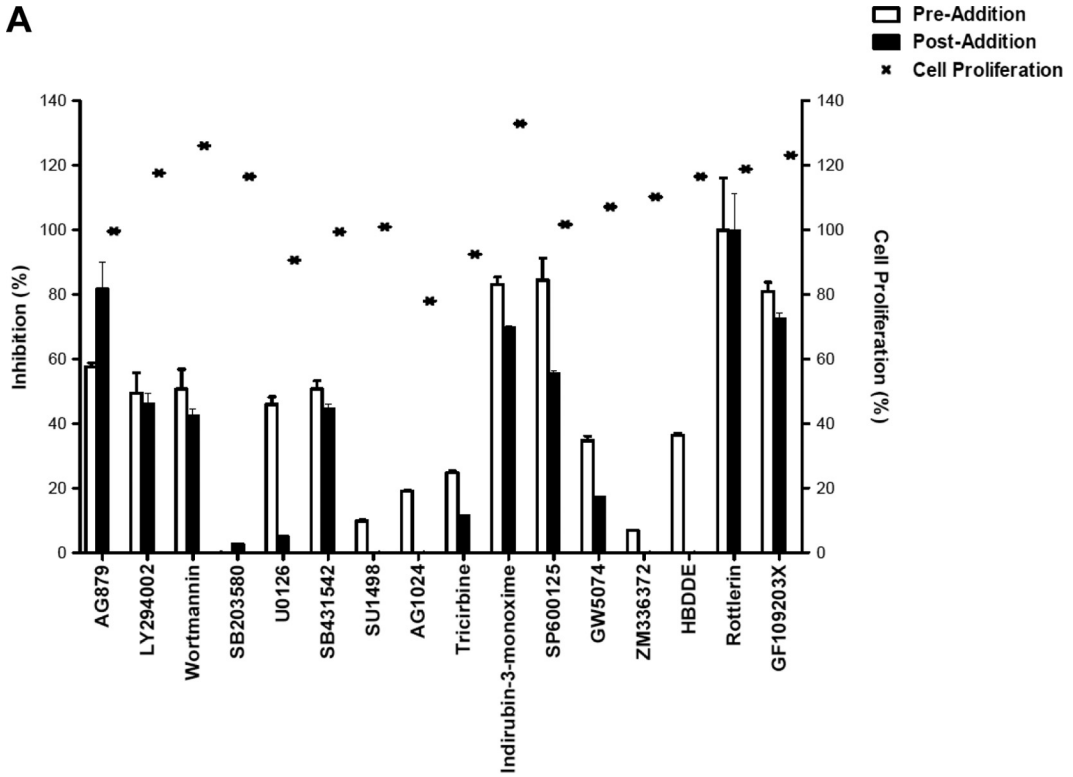

B

Inhibitor	Inhibition (%)		Cell Proliferation
	Pre-Infection	Post-Infection	
AG879	57.6	81.6	99.6
LY294002	49.4	46.0	117.6
Wortmannin	50.6	42.5	126.0
SB203580	0.0	2.5	116.5
U0126	45.9	4.9	90.6
SB431542	50.7	44.5	99.4
SU1498	9.8	0.0	100.9
AG1024	19.1	0.0	77.9
Tricirbine	24.9	11.4	92.4
Indirubin-3-monoxime	83.1	69.6	132.9
SP600125	84.4	55.3	101.7
GW5074	34.7	17.2	107.1
ZM336372	7.0	0.0	110.2
HBDDE	36.3	0.0	116.5
Rottlerin	99.8	99.8	118.8
GF109203X	80.8	72.4	123.1

FIG 4 Select kinase inhibitors specifically inhibit EBOV replication in hepatocytes. HUH7 cells were pretreated with the indicated kinase inhibitors (10 μM) for 1 h prior to infection (pretreatment) or 1 h postinfection with EBOV-GFP (MOI, 3). Fluorescence was assessed 24 h postinfection. Inhibition of infection (represented by bars) was calculated by comparing GFP-positive cells to total cells (DAPI stained). Data are representative of three independent experiments ± SD. Cell proliferation (represented by the line graph) was assessed using uninfected HUH7 cells treated with the indicated kinase inhibitors (10 μM) for 24 h. WST-1 reagent was added at the 24-h time point, and absorbance was measured at 450 nm in a multiwall plate reader 1 h post-WST-1 reagent addition. Data are presented as the means from three independent experiments. Graphical (A) and tabular (B) format of kinase inhibitor and cell viability results.

specifically modulated TGF-β-mediated signaling in a temporal fashion. Further, we demonstrated that TGF-β-mediated signaling responses were highly overrepresented 1 and 24 h p.i., TGF-β formed central nodes in the top functional networks associated with these time points, and TGF-β1 secretion was significantly induced from EBOV-infected cells compared to mock-infected control cells. Importantly, we observed a similar stimulatory effect on TGF-beta-mediated signaling responses in hepatocytes after infection with either crude virus preparations or with purified virus, speaking against a modulatory effect of exogenous stimula-

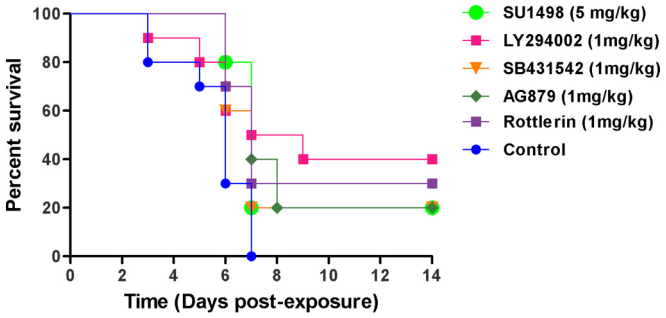

FIG 5 Inhibition of VEGF, NGF, PI3K, or PKC signaling pathways reduces lethality in EBOV infection. BALB/c mice were infected by intraperitoneal administration of mouse-adapted EBOV followed by intraperitoneal administration of kinase inhibitor 1 h later. A single administration of kinase inhibitor was given daily until day 5 postinfection.

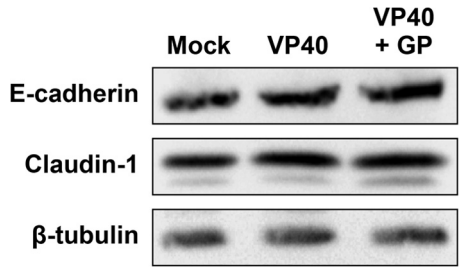

FIG 7 Ebola virus-like particles do not induce EMT-like phenotypic changes in hepatocytes. EBOV-like particles were constructed from VP40 or VP40 and GP viral proteins and quantified by electron microscopy. HUH7 cells were treated with virus-like particles (MOI, 3) or mock treated for 1 h, followed by washing. Cells were harvested 24 h postinfection and analyzed by Western blotting.

tory molecules potentially present in the crude virus preparations and providing further evidence for a critical role of this process during EBOV infection. Recently, Zhao and colleagues reported that SARS-CoV modulates TGF-β-mediated signaling, resulting in the attenuation of apoptosis and promotion of tissue fibrosis (57). In addition, it also has been shown that hepatitis C virus (HCV) infection alone or coinfection of HCV and human immunodeficiency virus 1 resulted in the upregulation of TGF-β-regulated genes and enhancement of HCV infection (58). Although a defined role for TGF-β-mediated signaling responses in EBOV pathogenesis has not been established, a potential role for TGF-β in filovirus infection has been suggested (59), and it was recently shown that TGF-β gene expression was temporally modulated in EBOV-infected Syrian golden hamsters hepatocytes (60).

To provide biological context to our observations, we examined specific cell markers that are associated with the modulation of TGF-β-mediated signaling responses and demonstrated that EBOV infection results in distinct local effects in hepatocytes. In addition to pleiotropic regulatory effects on broad cellular responses, TGF-β also can influence the phenotypic characteristics of cells, including those with epithelial or fibroblast morphologies. TGF-β has been show to promote EMT in epithelial cells and hepatocytes, resulting in the disassembly of tight junctions, modulation of the expression of specific cell proteins, and increased migratory and invasive properties (48). Although EMT has been investigated primarily for its role in embryonic development and tumor progression (61), there is increasing precedent for a broader role in microbial pathogenesis and wound healing (47,

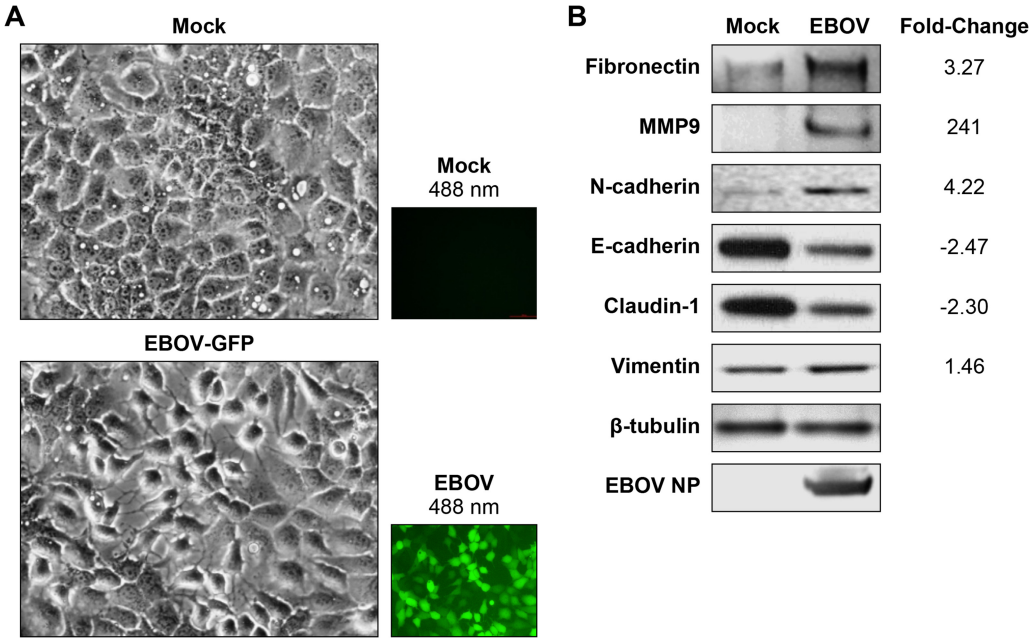

FIG 6 EBOV infection of hepatocytes induces markers of epithelium-to-mesenchyme transition. HUH7 cells were infected with EBOV-GFP or were mock infected (MOI, 3) for 24 h. (A) EBOV-GFP induced morphological changes in HUH7 cells, including reduced cell-cell contact, elongation, and spindle-like formation 24 h postinfection. (B) Western blot analysis of EBOV-infected HUH7 cell markers associated with EMT. EBOV infection resulted in the induction of fibronectin, matrix-metalloproteinase 9, and N-cadherin and the repression of E-cadherin, β-catenin, and claudin-1 expression. β-Tubulin is shown as a loading control, and EBOV NP is shown as a control for viral infection. Values for fold change differences in expression are displayed as EBOV levels relative to those of mock infection following normalization based on β-tubulin.

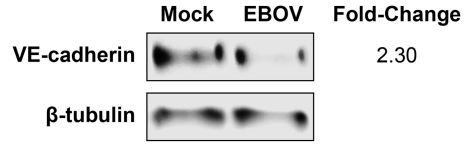

FIG 8 Phosphorylation state of TGF-β downstream regulators in response to EBOV infection in hepatocytes. HUH7 cells were infected with EBOV or were mock infected (MOI, 3) for 24 h. Downstream signaling intermediates from the TGF-β signaling pathway were analyzed with phospho-specific antibodies. EBOV infection resulted in the upregulated phosphorylation of TAK1, SMAD3, ERK1/2, and p38 compared to results for the mock-infected cells. JNK1/2 phosphorylation was downregulated in EBOV-infected cells compared to levels in the mock-infected controls. Values for fold change differences in expression are displayed as EBOV results relative to those of mock treatment following normalization based on β-tubulin.

62). EBOV infection resulted in the modulation of multiple cellular markers common to mesenchyme-like transition (including upregulation of N-cadherin, fibronectin, and MMP9 and downregulation of E-cadherin and claudin-1). Further, infection of human hepatocytes with purified EBOV resulted in the upregulation of several TGF-β-regulated signaling pathways, including those related to EMT. We also demonstrated that phosphorylation of ERK1/2, p38 MAPK, SMAD3, and TAK1 was increased in EBOV-infected cells compared to levels under mock treatment conditions 24 h p.i., providing evidence for a role of these downstream signaling events in EBOV-induced TGF-β signaling. Taken together, these results highlight a novel biological role for the modulation of TGF-β-mediated signaling during EBOV infection. For example, cells undergoing EMT can transverse into the vasculature through intravasation (48). As it has been speculated that EBOV-infected fibroblasts spread viral progeny to distant sites through cell protrusions (63), the modulation of mesenchyme-like cellular markers in EBOV-infected hepatocytes could enhance viral spread in the liver. We also have shown that EBOV infection modulated VEGF secretion and VEGF-mediated signaling responses in infected hepatocytes, and regulatory roles for TGF-β in VEGF secretion from epithelial cells, angiogenesis, and vascular permeability have been reported (41, 42, 64, 65). Thus, the activation of TGF-β-mediated signaling during EBOV infection may contribute to viral pathogenesis through both local phenotypic effects on hepatocytes and secondary effects, including changes to vascular permeability, resulting from the induction of VEGF or other TGF-β-regulated cytokines, chemokines, and growth factors. In support of this, influenza A virus infection results in the modulation of epithelial cell chemokine/cytokine secretion with subsequent damage to the epithelium-endothelium barrier (66). Thus, we have proposed a model for the role of TGF-β-mediated signaling modulation during the course of EBOV infection (Fig. 10). We postulate that the infection of hepatocytes by EBOV results in the activation of two events: (i) the local release of cytokines, notably TGF-β and VEGF (and, to a lesser extent, MCP-1, Gro-α, and IL-8), and (ii) the modulation of EMT-specific cell marker expression within the infected cells. The local release of cytokines could trigger the disruption of the adherens junctions in proximal blood vessels or capillaries with the loss of endothelial cell integrity, as described for influenza A virus infection (66). Indeed, treatment of HUVECs with virus-free conditioned media from EBOV-infected HUH7 cells resulted in reduced expression of VE-cadherin, a primary marker of endothelial cell integrity.

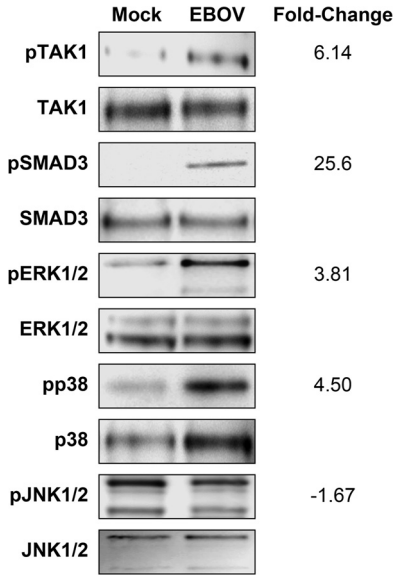

FIG 9 VE-cadherin expression is downregulated in HUVECs following treatment with virus-free conditioned media from EBOV-infected HUH7 cells. HUVECs were treated with virus-free conditioned media from EBOV-infected HUH7 cells or mock-infected cells (diluted 1:1 with fresh EGM-2 media) for 24 h. Cells were harvested 24 h postinfection and analyzed by Western blotting. Values for fold change differences in expression are displayed as EBOV values relative to those of mock treatment following normalization based on β-tubulin.

The latter events could contribute to EBOV infection and pathogenesis through permeabilization of the vasculature and release of infected hepatocytes and/or virus into the bloodstream, and these tenets will be examined in future investigations.

We also investigated the roles for modulation of downstream PI3K/AKT, PKC, and ERK/MAPK signaling during EBOV infection, and many of these signaling intermediates also have been demonstrated to regulate EMT (67). Selective inhibition of PI3K, but not AKT, resulted in inhibition of EBOV replication when added pre- or postinfection, suggesting an important role for PI3K in EBOV infection. This also was reflected in our kinome data, as PI3K phosphorylation was significantly increased and AKT phosphorylation significantly decreased in EBOV-infected cells compared to mock-infected cells. Although inhibition of multiple PKC isoforms resulted in reduced EBOV replication, our data suggested a pivotal role for PKCδ, as demonstrated by the inhibitory activities of rottlerin and GF109203X when added pre- or postinfection. In accordance with this, Bakin and colleagues have demonstrated that PKC-mediated activation of MAPK signaling can induce EMT (68). In addition, the administration of kinase inhibitors selected from our *in vitro* data, in particular those that inhibited EBOV infection, whether added pre- or postinfection, reduced lethality in a mouse model of EBOV disease. The delay in disease progression and reduced lethality in our animal model support a role for these signaling events during EBOV infection *in vivo*. The inhibition of downstream PI3K/AKT and PKC signaling resulted in a greater reduction in EBOV lethality and likely reflects the redundancy of the PI3K/AKT and PKC signaling pathways across multiple signaling networks, including TGF-β, VEGF, and NGF, for which only a marginally protective effect was demonstrated. Although the inhibition of specific cell signaling events did not result in complete protection from EVD

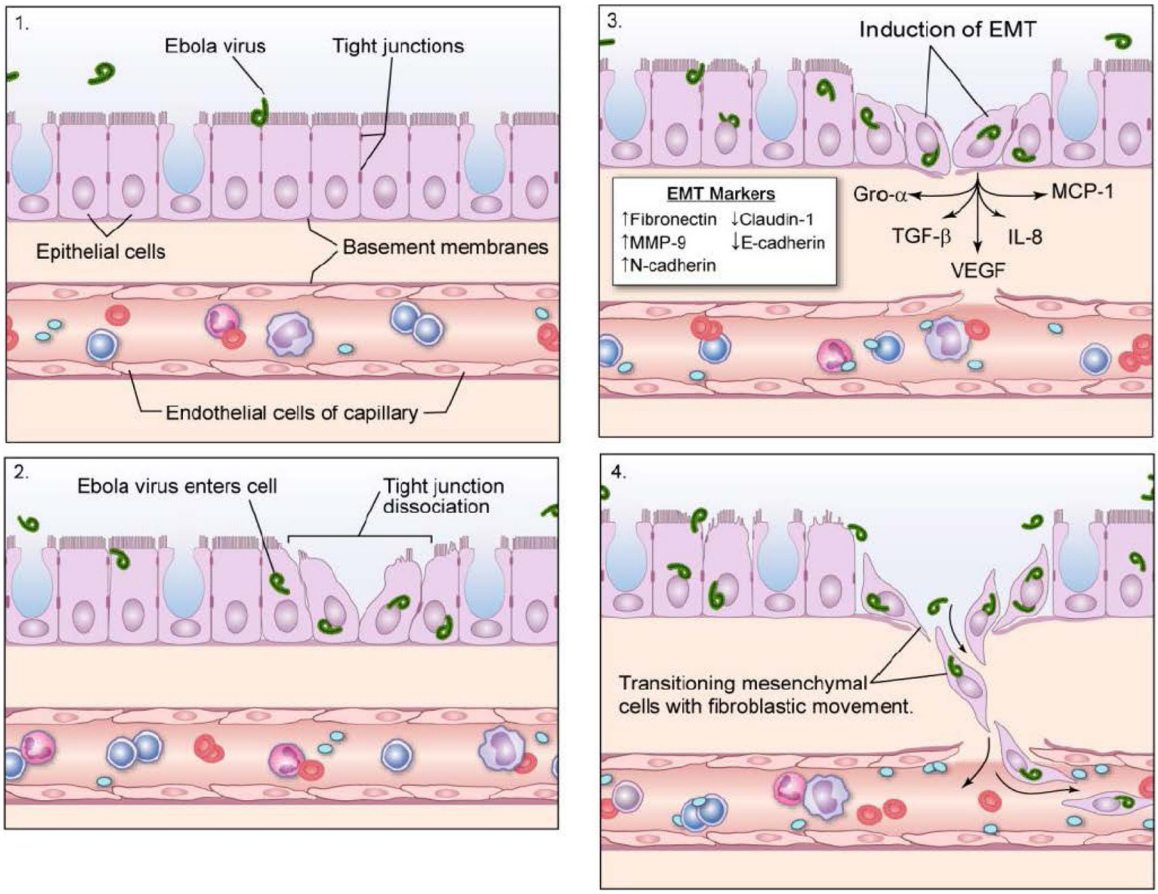

FIG 10 Potential roles for TGF-β signaling and mesenchymal cell marker expression modulation during EBOV infection. The proposed model of EBOV-mediated TGF-β activation and modulation of mesenchyme-like cell marker expression occurs over four stages: stage 1, Ebola virus infects epithelial cells; stage 2, dissociation of cell-to-cell contacts; stage 3, infected cells release various cytokines and chemokines that can have autocrine or paracrine effects, with concomitant modulation of expression of mesenchymal cell marker from epithelium-like to mesenchyme-like; stage 4, loss of epithelial cell integrity, increased motility of infected mesenchyme-like cells, and release of cytokines and chemokines with downstream effects on the surrounding vasculature (i.e., disruption of adherens junctions and downregulation of VE-cadherin) contribute to EBOV pathogenesis.

progression, the goal of this experiment was not to test full therapeutic efficacy but rather potential roles in disease pathogenesis. Thus, these results may warrant additional studies that explore more optimized treatment regimens or drug combinations to assess therapeutic efficacy. Interestingly, SU1498, a selective VEGF inhibitor, reduced lethality *in vivo*, in contrast to the lack of inhibitory activity of SU1498 on EBOV infection *in vitro*. This may reflect a protective effect from secreted VEGF from infected hepatocytes, as well as broader roles for the VEGF signaling pathway in EBOV infection. Collectively, this highlights the multiple roles for PI3K/AKT and PKC during the course of EBOV infection.

This investigation demonstrates the utility of temporal kinome analysis for identifying specific host signaling networks or pathways modulated during infection and their potential biological roles in disease pathogenesis. Our investigation has provided pertinent information regarding the host responses of hepatocytes to EBOV infection and has demonstrated a role for the modulation of TGF-β-mediated signaling pathways in hepatocytes during the course of EBOV infection. In addition, we have confirmed that TGF-β and associated downstream signaling pathways contribute to EBOV infection *in vitro* and *in vivo*. Lastly, we have identified a novel mechanism through which EBOV infection of hepatocytes may contribute to pathogenesis locally and systemically through the modulation of specific cellular markers, reminiscent of mesenchyme-like transition. Taken together, we demonstrate the power of kinomics for identifying specific cell signaling events and their role in molecular pathogenesis through a global survey of host responses and, importantly, for the identification of novel host targets that may be of therapeutic interest.

ACKNOWLEDGMENTS

This study was supported in part by the NIAID Division of Intramural Research. We also thank Lydia Kibiuk (NIH Medical Arts & Design) for her illustrations and Catherine Jett for her contributions to the Bioplex analysis. We thank Jens Kuhn for critical review of the manuscript.

J.K. performed this work partially as an employee of Battelle Memorial Institute, and V.W.-J. performed this work partially as an employee of Tunnell Government Services, Inc., both under Battelle Memorial Institute's prime contract with NIAID, contract no. HHSN272200700016I.

The contents of this publication do not necessarily reflect the views or policies of the U.S. Department of Health and Human Services or of the institutions and companies affiliated with the authors. The views and conclusions contained in this document are those of the authors and should not be interpreted as necessarily representing the official policies, either expressed or implied, of the U.S. Department of Homeland Secu-

rity. In no event shall the DHS, NBACC, or Battelle National Biodefense Institute (BNBI) have any responsibility or liability for any use, misuse, inability to use, or reliance upon the information contained herein. The Department of Homeland Security does not endorse any products or commercial services mentioned in this publication.

REFERENCES

1. **Kuhn J, Becker S, Ebihara H, Geisbert TW, Jahrling PB, Kawaoka Y, Netesov SV, Nichol ST, Peters CJ, Volchkov VE, Ksiazek TG.** 2012. *Filoviridae*, p 665–671. *In* King AMQ, Adams MJ, Carstens EB, Lefkowitz EJ (ed), Virus taxonomy: classification and nomenclature of viruses. Ninth report of the International Committee on Taxonomy of Viruses. Academic Press, London, United Kingdom.
2. **Feldmann H, Geisbert TW.** 2011. Ebola haemorrhagic fever. Lancet **377:**849–862. http://dx.doi.org/10.1016/S0140-6736(10)60667-8.
3. **Gatherer D.** 2 May 2014. The 2014 Ebola virus disease outbreak in west Africa. J. Gen. Virolhttp://dx.doi.org/10.1099/vir.0.067199-0.
4. **Wasswa H.** 2012. Uganda gears up to contain Ebola epidemic as fears of spread cause panic. BMJ **345:**e5210. http://dx.doi.org/10.1136/bmj.e5210.
5. **Anonymous.** 2009. Imported case of Marburg hemorrhagic fever-Colorado, 2008. MMWR Morb. Mortal. Wkly. Rep. **58:**1377–1381.
6. **Timen A, Koopmans MP, Vossen AC, van Doornum GJ, Gunther S, van den Berkmortel F, Verduin KM, Dittrich S, Emmerich P, Osterhaus AD, van Dissel JT, Coutinho RA.** 2009. Response to imported case of Marburg hemorrhagic fever, the Netherlands. Emerg. Infect. Dis. **15:** 1171–1175. http://dx.doi.org/10.3201/eid1508.090015.
7. **Hoenen T, Groseth A, Feldmann H.** 2012. Current Ebola vaccines. Expert Opin. Biol. Ther. **12:**859–872. http://dx.doi.org/10.1517/14712598.2012.685152.
8. **Kondratowicz AS, Maury WJ.** 2012. Ebolavirus: a brief review of novel therapeutic targets. Future Microbiol. **7:**1–4. http://dx.doi.org/10.2217/fmb.11.110.
9. **Takada A, Kawaoka Y.** 2001. The pathogenesis of Ebola hemorrhagic fever.TrendsMicrobiol.**9:**506–511.http://dx.doi.org/10.1016/S0966-842X(01)02201-6.
10. **Aleksandrowicz P, Wolf K, Falzarano D, Feldmann H, Seebach J, Schnittler H.** 2008. Viral haemorrhagic fever and vascular alterations. Hamostaseologie **28:**77–84.
11. **Mahanty S, Hutchinson K, Agarwal S, McRae M, Rollin PE, Pulendran B.** 2003. Cutting edge: impairment of dendritic cells and adaptive immunity by Ebola and Lassa viruses. J. Immunol. **170:**2797–2801. http://dx.doi.org/10.4049/jimmunol.170.6.2797.
12. **Rubins KH, Hensley LE, Wahl-Jensen V, Daddario DiCaprio KM, Young HA, Reed DS, Jahrling PB, Brown PO, Relman DA, Geisbert TW.** 2007. The temporal program of peripheral blood gene expression in the response of nonhuman primates to Ebola hemorrhagic fever. Genome Biol. **8:**R174. http://dx.doi.org/10.1186/gb-2007-8-8-r174.
13. **Villinger F, Rollin PE, Brar SS, Chikkala NF, Winter J, Sundstrom JB, Zaki SR, Swanepoel R, Ansari AA, Peters CJ.** 1999. Markedly elevated levels of interferon (IFN)-gamma, IFN-alpha, interleukin (IL)-2, IL-10, and tumor necrosis factor-alpha associated with fatal Ebola virus infection. J. Infect. Dis. **179**(Suppl 1)**:**S188–S191.
14. **Baize S, Leroy EM, Georges AJ, Georges-Courbot MC, Capron M, Bedjabaga I, Lansoud-Soukate J, Mavoungou E.** 2002. Inflammatory responses in Ebola virus-infected patients. Clin. Exp. Immunol. **128:**163–168. http://dx.doi.org/10.1046/j.1365-2249.2002.01800.x.
15. **Geisbert TW, Young HA, Jahrling PB, Davis KJ, Larsen T, Kagan E, Hensley LE.** 2003. Pathogenesis of Ebola hemorrhagic fever in primate models: evidence that hemorrhage is not a direct effect of virus-induced cytolysis of endothelial cells. Am. J. Pathol. **163:**2371–2382. http://dx.doi.org/10.1016/S0002-9440(10)63592-4.
16. **Gupta M, Mahanty S, Ahmed R, Rollin PE.** 2001. Monocyte-derived human macrophages and peripheral blood mononuclear cells infected with Ebola virus secrete MIP-1alpha and TNF-alpha and inhibit poly-IC-induced IFN-alpha in vitro. Virology **284:**20–25. http://dx.doi.org/10.1006/viro.2001.0836.
17. **Hensley LE, Young HA, Jahrling PB, Geisbert TW.** 2002. Proinflammatory response during Ebola virus infection of primate models: possible involvement of the tumor necrosis factor receptor superfamily. Immunol. Lett. **80:**169–179. http://dx.doi.org/10.1016/S0165-2478(01)00327-3.
18. **Schnittler HJ, Feldmann H.** 1999. Molecular pathogenesis of filovirus infections: role of macrophages and endothelial cells. Curr. Topics Microbiol. Immunol. **235:**175–204.
19. **Bowen ET, Platt GS, Simpson DI, McArdell LB, Raymond RT.** 1978. Ebola haemorrhagic fever: experimental infection of monkeys. Trans. R. Soc. Trop. Med. Hyg. **72:**188–191. http://dx.doi.org/10.1016/0035-9203(78)90058-5.
20. **Ellis DS, Simpson IH, Francis DP, Knobloch J, Bowen ET, Lolik P, Deng IM.** 1978. Ultrastructure of Ebola virus particles in human liver. J. Clin. Pathol. **31:**201–208. http://dx.doi.org/10.1136/jcp.31.3.201.
21. **Stroher U, West E, Bugany H, Klenk HD, Schnittler HJ, Feldmann H.** 2001. Infection and activation of monocytes by Marburg and Ebola viruses. J. Virol. **75:**11025–11033. http://dx.doi.org/10.1128/JVI.75.22.11025-11033.2001.
22. **Wyers M, Formenty P, Cherel Y, Guigand L, Fernandez B, Boesch C, Le Guenno B.** 1999. Histopathological and immunohistochemical studies of lesions associated with Ebola virus in a naturally infected chimpanzee. J. Infect. Dis. **179**(Suppl 1)**:**S54–S59.
23. **Hartman AL, Ling L, Nichol ST, Hibberd ML.** 2008. Whole-genome expression profiling reveals that inhibition of host innate immune response pathways by Ebola virus can be reversed by a single amino acid change in the VP35 protein. J. Virol. **82:**5348–5358. http://dx.doi.org/10.1128/JVI.00215-08.
24. **Kash JC, Muhlberger E, Carter V, Grosch M, Perwitasari O, Proll SC, Thomas MJ, Weber F, Klenk HD, Katze MG.** 2006. Global suppression of the host antiviral response by Ebola- and Marburgviruses: increased antagonism of the type I interferon response is associated with enhanced virulence. J. Virol. **80:**3009–3020. http://dx.doi.org/10.1128/JVI.80.6.3009-3020.2006.
25. **Wahl-Jensen V, Kurz S, Feldmann F, Buehler LK, Kindrachuk J, DeFilippis V, da Silva Correia J, Fruh K, Kuhn JH, Burton DR, Feldmann H.** 2011. Ebola virion attachment and entry into human macrophages profoundly effects early cellular gene expression. PLoS Negl. Trop. Dis. **5:**e1359. http://dx.doi.org/10.1371/journal.pntd.0001359.
26. **Kindrachuk J, Napper S.** 2013. Probing the kinome for biomakers and therapeutic targets: peptide arrays for global phosphorylation-mediated signal transduction. *In* Horvatovich P, Bischoff R (ed), Comprehensive biomarker discovery and validation for clinical applications. Royal Society of Chemistry, Cambridge, United Kingdom.
27. **Piersma SR, Labots M, Verheul HM, Jimenez CR.** 2010. Strategies for kinome profiling in cancer and potential clinical applications: chemical proteomics and array-based methods. Anal. Bioanal Chem. **397:**3163–3171. http://dx.doi.org/10.1007/s00216-010-3784-7.
28. **Arsenault R, Griebel P, Napper S.** 2011. Peptide arrays for kinome analysis: new opportunities and remaining challenges. Proteomics **11:** 4595–4609. http://dx.doi.org/10.1002/pmic.201100296.
29. **Kindrachuk J, Arsenault R, Kusalik A, Kindrachuk KN, Trost B, Napper S, Jahrling PB, Blaney JE.** 2012. Systems kinomics demonstrates Congo Basin monkeypox virus infection selectively modulates host cell signaling responses as compared to West African monkeypox virus. Mol. Cell. Proteomics **11:**M111.015701. http://dx.doi.org/10.1074/mcp.M111.015701.
30. **Ryabchikova EI, Kolesnikova LV, Luchko SV.** 1999. An analysis of features of pathogenesis in two animal models of Ebola virus infection. J. Infect. Dis. **179**(Suppl 1)**:**S199–S202. http://dx.doi.org/10.1086/514293.
31. **U.S. Department of Health and Human Services.** 2009. Biosafety in microbiological and biomedical laboratories, 5th ed. U.S. Department of Health and Human Services, Washington, DC.
32. **Li Y, Arsenault RJ, Trost B, Slind J, Griebel PJ, Napper S, Kusalik A.** 2012. A systematic approach for analysis of peptide array kinome data. Sci. Signal. **5:**pl2. http://dx.doi.org/10.1126/scisignal.2002429.
33. **Huber W, von Heydebreck A, Sultmann H, Poustka A, Vingron M.** 2002. Variance stabilization applied to microarray data calibration and to the quantification of differential expression. Bioinformatics **18**(Suppl 1)**:** S96–S104. http://dx.doi.org/10.1093/bioinformatics/18.suppl_1.S96.
34. **Trost B, Kindrachuk J, Maattanen P, Napper S, Kusalik A.** 2013. PIIKA 2: an expanded, web-based platform for analysis of kinome microarray data. PLoS One **8:**e80837. http://dx.doi.org/10.1371/journal.pone.0080837.
35. **McQuitty L.** 1996. Similarity analysis by reciprocal pairs for discrete and continuous data. Educ. Psychol. Meas. **26:**825–831.
36. **Dudley AC, Thomas D, Best J, Jenkins A.** 2005. A VEGF/JAK2/STAT5 axis may partially mediate endothelial cell tolerance to hypoxia. Biochem. J. **390:**427–436. http://dx.doi.org/10.1042/BJ20050351.
37. **Groseth A, Hoenen T, Alimonti JB, Zielecki F, Ebihara H, Theriault S, Stroher U, Becker S, Feldmann H.** 2007. In vitro evaluation of antisense RNA efficacy against filovirus infection, by use of reverse genetics. J. Infect. Dis. **196**(Suppl 2)**:**S382–S389. http://dx.doi.org/10.1086/520604.

38. **National Research Council.** 2011. Guide for the care and use of laboratory animals, 8th ed. National Academies Press, Washington, DC.
39. **Arsenault RJ, Li Y, Bell K, Doig K, Potter A, Griebel PJ, Kusalik A, Napper S.** 2012. Mycobacterium avium subsp. paratuberculosis inhibits gamma interferon-induced signaling in bovine monocytes: insights into the cellular mechanisms of Johne's disease. Infect. Immun. **80:**3039-3048. http://dx.doi.org/10.1128/IAI.00406-12.
40. **Lynn DJ, Winsor GL, Chan C, Richard N, Laird MR, Barsky A, Gardy JL, Roche FM, Chan TH, Shah N, Lo R, Naseer M, Que J, Yau M, Acab M, Tulpan D, Whiteside MD, Chikatamarla A, Mah B, Munzner T, Hokamp K, Hancock RE, Brinkman FS.** 2008. InnateDB: facilitating systems-level analyses of the mammalian innate immune response. Mol. Syst. Biol. **4:**218. http://dx.doi.org/10.1038/msb.2008.55.
41. **Donovan D, Harmey JH, Toomey D, Osborne DH, Redmond HP, Bouchier-Hayes DJ.** 1997. TGF beta-1 regulation of VEGF production by breast cancer cells. Ann. Surg. Oncol. **4:**621–627. http://dx.doi.org/10.1007/BF02303745.
42. **Sanchez-Elsner T, Botella LM, Velasco B, Corbi A, Attisano L, Bernabeu C.** 2001. Synergistic cooperation between hypoxia and transforming growth factor-beta pathways on human vascular endothelial growth factor gene expression. J. Biol. Chem. **276:**38527–38535. http://dx.doi.org/10.1074/jbc.M104536200.
43. **Bray M, Davis K, Geisbert T, Schmaljohn C, Huggins J.** 1998. A mouse model for evaluation of prophylaxis and therapy of Ebola hemorrhagic fever. J. Infect. Dis. **178:**651–661. http://dx.doi.org/10.1086/515386.
44. **Kaimori A, Potter J, Kaimori JY, Wang C, Mezey E, Koteish A.** 2007. Transforming growth factor-beta1 induces an epithelial-to-mesenchymal transition state in mouse hepatocytes in vitro. J. Biol. Chem. **282:**22089–22101. http://dx.doi.org/10.1074/jbc.M700998200.
45. **Zeisberg M, Yang C, Martino M, Duncan MB, Rieder F, Tanjore H, Kalluri R.** 2007. Fibroblasts derive from hepatocytes in liver fibrosis via epithelial to mesenchymal transition. J. Biol. Chem. **282:**23337–23347. http://dx.doi.org/10.1074/jbc.M700194200.
46. **Li MO, Wan YY, Sanjabi S, Robertson AK, Flavell RA.** 2006. Transforming growth factor-beta regulation of immune responses. Annu. Rev. Immunol. **24:**99–146. http://dx.doi.org/10.1146/annurev.immunol.24.021605.090737.
47. **Borthwick LA, Sunny SS, Oliphant V, Perry J, Brodlie M, Johnson GE, Ward C, Gould K, Corris PA, De Soyza A, Fisher AJ.** 2011. Pseudomonas aeruginosa accentuates epithelial-to-mesenchymal transition in the airway. Eur. Respir. J. **37:**1237–1247. http://dx.doi.org/10.1183/09031936.00088410.
48. **Xu J, Lamouille S, Derynck R.** 2009. TGF-beta-induced epithelial to mesenchymal transition. Cell Res. **19:**156–172. http://dx.doi.org/10.1038/cr.2009.5.
49. **Liu S, Yang W, Shen L, Turner JR, Coyne CB, Wang T.** 2009. Tight junction proteins claudin-1 and occludin control hepatitis C virus entry and are downregulated during infection to prevent superinfection. J. Virol. **83:**2011–2014. http://dx.doi.org/10.1128/JVI.01888-08.
50. **Borthwick LA, Gardner A, De Soyza A, Mann DA, Fisher AJ.** 2012. Transforming growth factor-beta1 (TGF-beta1) driven epithelial to mesenchymal transition (EMT) is accentuated by tumour necrosis factor alpha (TNFalpha) via crosstalk between the SMAD and NF-kappaB pathways. Cancer Microenviron. **5:**45–57. http://dx.doi.org/10.1007/s12307-011-0080-9.
51. **Kuhn JH.** 2008. Filoviruses. A compendium of 40 years of epidemiological, clinical, and laboratory studies. Arch. Virol. Suppl. **20:**13–360.
52. **Davis KJ, Anderson AO, Geisbert TW, Steele KE, Geisbert JB, Vogel P, Connolly BM, Huggins JW, Jahrling PB, Jaax NK.** 1997. Pathology of experimental Ebola virus infection in African green monkeys. Involvement of fibroblastic reticular cells. Arch. Pathol. Lab. Med. **121:**805–819.
53. **Ito H, Watanabe S, Takada A, Kawaoka Y.** 2001. Ebola virus glycoprotein: proteolytic processing, acylation, cell tropism, and detection of neutralizing antibodies. J. Virol. **75:**1576–1580. http://dx.doi.org/10.1128/JVI.75.3.1576-1580.2001.
54. **Johnson E, Jaax N, White J, Jahrling P.** 1995. Lethal experimental infections of rhesus monkeys by aerosolized Ebola virus. Int. J. Exp. Pathol. **76:**227–236.
55. **Ryabchikova E, Kolesnikova L, Smolina M, Tkachev V, Pereboeva L, Baranova S, Grazhdantseva A, Rassadkin Y.** 1996. Ebola virus infection in guinea pigs: presumable role of granulomatous inflammation in pathogenesis. Arch. Virol. **141:**909–921. http://dx.doi.org/10.1007/BF01718165.
56. **Steele KE, Anderson AO, Mohamadzadeh M.** 2009. Fibroblastic reticular cell infection by hemorrhagic fever viruses. Immunotherapy **1:**187–197. http://dx.doi.org/10.2217/1750743X.1.2.187.
57. **Zhao X, Nicholls JM, Chen YG.** 2008. Severe acute respiratory syndrome-associated coronavirus nucleocapsid protein interacts with Smad3 and modulates transforming growth factor-beta signaling. J. Biol. Chem. **283:**3272–3280. http://dx.doi.org/10.1074/jbc.M708033200.
58. **Zhang X, Daucher M, Baeza J, Kim CW, Russell R, Kottilil S.** 2012. Human immunodeficiency virus enhances hepatitis C virus replication by differential regulation of IFN and TGF family genes. J. Med. Virol. **84:**1344–1352. http://dx.doi.org/10.1002/jmv.23315.
59. **Mohamadzadeh M.** 2009. Potential factors induced by filoviruses that lead to immune suppression. Curr. Mol. Med. **9:**174–185. http://dx.doi.org/10.2174/156652409787581628.
60. **Ebihara H, Zivcec M, Gardner D, Falzarano D, Lacasse R, Rosenke R, Long D, Haddock E, Fischer E, Kawaoka Y, Feldmann H.** 2012. A Syrian golden hamster model recapitulating ebola hemorrhagic fever. J. Infect. Dis. **207:**306–318. http://dx.doi.org/10.1093/infdis/jis626.
61. **Thiery JP.** 2002. Epithelial-mesenchymal transitions in tumour progression. Nat. Rev. Cancer **2:**442–454. http://dx.doi.org/10.1038/nrc822.
62. **Zeisberg M, Hanai J, Sugimoto H, Mammoto T, Charytan D, Strutz F, Kalluri R.** 2003. BMP-7 counteracts TGF-beta1-induced epithelial-to-mesenchymal transition and reverses chronic renal injury. Nat. Med. **9:**964–968. http://dx.doi.org/10.1038/nm888.
63. **Olejnik J, Ryabchikova E, Corley RB, Muhlberger E.** 2011. Intracellular events and cell fate in filovirus infection. Viruses **3:**1501–1531. http://dx.doi.org/10.3390/v3081501.
64. **Hassan M, Selimovic D, Ghozlan H, Abdel-Kader O.** 2009. Hepatitis C virus core protein triggers hepatic angiogenesis by a mechanism including multiple pathways. Hepatology **49:**1469–1482. http://dx.doi.org/10.1002/hep.22849.
65. **ten Dijke P, Arthur HM.** 2007. Extracellular control of TGFbeta signalling in vascular development and disease. Nat. Rev. Mol. Cell Biol. **8:**857–869. http://dx.doi.org/10.1038/nrm2262.
66. **Short KR, Kroeze EJ, Fouchier RA, Kuiken T.** 2014. Pathogenesis of influenza-induced acute respiratory distress syndrome. Lancet Infect. Dis. **14:**57–69. http://dx.doi.org/10.1016/S1473-3099(13)70286-X.
67. **Bakin AV, Tomlinson AK, Bhowmick NA, Moses HL, Arteaga CL.** 2000. Phosphatidylinositol 3-kinase function is required for transforming growth factor beta-mediated epithelial to mesenchymal transition and cell migration. J. Biol. Chem. **275:**36803–36810. http://dx.doi.org/10.1074/jbc.M005912200.
68. **Bakin AV, Rinehart C, Tomlinson AK, Arteaga CL.** 2002. p38 mitogen-activated protein kinase is required for TGFbeta-mediated fibroblastic transdifferentiation and cell migration. J. Cell Sci. **115:**3193–3206.